2024 American Control Conference (ACC)
July 8-12, 2024. Toronto, Canada

Safety-critical Stabilization of Mixed Traffic by Pairs of CAVs

Chenguang Zhao[1], Tamas G. Molnar[2], Huan Yu[1,*]

***Abstract*— Connected and automated vehicles (CAVs) have been widely applied to vehicle-based traffic control in mixed-autonomy systems that consist of CAVs and human-driven vehicles (HVs). The control designs of CAVs allow them to drive smoothly, cooperate, and stabilize the flow of traffic. However, these controllers must also ensure safe behaviors for CAVs as well as consider their potential impact on the safety of following HVs. In this paper, we propose nonlinear controllers for a pair of CAVs that respond to each other whilst traveling amongst HVs. The controllers seek to stabilize traffic, while the safety of CAVs in terms of front-end collisions is formally guaranteed via control barrier functions. We analyze how the coordination of CAVs affects stability and safety in the mixed traffic system. The efficacy of the proposed controllers is demonstrated by numerical simulations.**

***Index Terms*— Connected and automated vehicle, mixed traffic, stability analysis, safety-critical control**

I. Introduction

Connected and automated vehicles (CAVs) have shown great potential in improving traffic systems from multiple aspects, such as increasing capacity, reducing emissions, and mitigating congestion. Before fully automated traffic becomes a reality, there will inevitably be a long transition period of mixed traffic, where CAVs co-exist with human-driven vehicles (HVs). Therefore, controller design for CAVs in mixed traffic has received considerable attention.

Both theory [5], [7] and field experiments [14] have shown that CAVs are effective in smoothing (stabilizing) traffic and reducing congestion. Multiple types of stabilizing controllers have been proposed to leverage the connectivity between CAVs [11], [13], [15], [16] in various traffic scenarios.

While improving the stability of mixed traffic is highly beneficial, it must be accomplished in a way that the safety of the individual CAVs is ensured. It has been shown that safety, especially avoiding front-end collisions, is one key index affecting the public acceptance of CAVs [6]. Control design methods that guarantee safety for CAVs include reachability analysis [1], [12], model predictive control [8], linear matrix inequalities [7], and control barrier functions (CBFs) [3], [17], [19]. Remarkably, CBFs have the flexibility to synthesize safety-critical controllers from pre-designed nominal controllers [2], [10] such as those stabilizing traffic. In our previous work [19], we leveraged this idea and utilized CBFs to develop safety-critical traffic control (STC) that enables a CAV to stabilize the traffic behind it while maintaining formal safety guarantees.

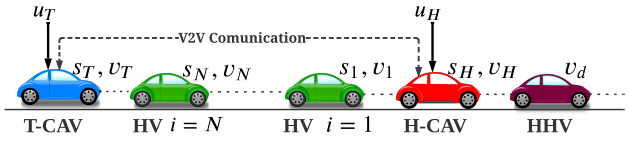

Fig. 1: The proposed framework for safety-critical stabilization of mixed-autonomy traffic consisting of connected automated vehicles (CAVs) and human-driven vehicles (HVs). A vehicle chain behind a head HV (HHV) is considered with a head CAV (H-CAV), N HVs and a tail CAV (T-CAV). The CAV pair is controlled such that they mitigate congestion while maintaining formal guarantees of safe driving.

The aforementioned controllers focus on a single CAV in mixed traffic. In practice, there may be multiple CAVs within each other's communication range, and well-designed interaction between them may further improve traffic systems. Controllers designed for multiple CAVs have shown success in stabilizing traffic and reducing congestion [4], [9], [15]. However, understanding the effect of the interaction between CAVs on safety and addressing how to coordinate CAVs to avoid collisions is still an open question.

In this paper, we propose safety-critical traffic controllers for multiple CAVs in mixed-autonomy traffic. Specifically, we consider a pair of CAVs that drive amongst HVs and respond to each other; see Fig 1. First, we design stabilizing controllers that allow the CAVs to mitigate congestion and ensure smooth traffic. By analyzing the underlying stability conditions, we derive stability charts and show that the response of the two CAVs to each other enhances the stability of mixed traffic. Second, we design safety-critical controllers for the two CAVs via CBFs to formally guarantee their safe driving behavior. We demonstrate by numerical simulations that, with the proper choice of control gains, the integration of the stabilizing traffic controller and CBFs achieves both string stability and front-end collision-free safety.

The rest of this paper is organized as follows. We formulate the dynamics of mixed-autonomy traffic with a CAV pair in Section II. In Section III, we design stabilizing traffic controllers based on stability charts. In Section IV, we utilize CBFs to design safety filters for the two CAVs, and analyze their safety and performance via numerical simulations.

II. Problem Formulation

We consider a vehicle chain consisting of two CAVs traveling in traffic as shown in Fig 1. The head CAV (H-CAV) follows some head vehicles and leads N following HVs indexed from 1 to N. The tail CAV (T-CAV) is at the end of the considered vehicle chain and follows HV-N.

[1] Chenguang Zhao and Huan Yu are with the Thrust of Intelligent Transportation, The Hong Kong University of Science and Technology (Guangzhou), Guangzhou, 511400, China. Huan Yu is also with the Department of Civil and Environmental Engineering, The Hong Kong University of Science and Technology, Hong Kong SAR, China.

[2] Tamas G. Molnar is with the Department of Mechanical Engineering, Wichita State University, Wichita, KS 67260, USA.

[*] Corresponding author: Huan Yu (huanyu@ust.hk)

HV dynamics: For HV-i, its speed $v_i \in \mathbb{R}$ and gap $s_i \in \mathbb{R}$ follow:

$$\dot{s}_i = v_{i-1} - v_i, \tag{1}$$
$$\dot{v}_i = F_i(s_i, v_i, \dot{s}_i), \tag{2}$$

where $v_{i-1} \in \mathbb{R}$ is the speed of its leader vehicle HV-$(i-1)$, and $F_i : \mathbb{R}^3 \to \mathbb{R}$ describes the driving strategy of HV-i, such as the optimal velocity model (OVM), or the intelligent driver model (IDM). For HV-1 that directly follows the head CAV, we use the notation $v_0 = v_{\rm H}$ to represent the speed of its leader, the head CAV.

CAV dynamics: For the two CAVs, their accelerations are controlled by the designed controller. For the head CAV (H-CAV), its gap $s_{\rm H} \in \mathbb{R}$ and speed $v_{\rm H} \in \mathbb{R}$ are governed as:

$$\dot{s}_{\rm H} = v_{\rm d} - v_{\rm H}, \tag{3}$$
$$\dot{v}_{\rm H} = u_{\rm H}, \tag{4}$$

with $v_{\rm d} \in \mathbb{R}$ being the speed of the head HV (HHV) ahead of the H-CAV, and $u_{\rm H} \in \mathbb{R}$ being the control input for the H-CAV. For the tail CAV (T-CAV), the dynamics of its gap $s_{\rm T} \in \mathbb{R}$ and speed $v_{\rm T} \in \mathbb{R}$ are:

$$\dot{s}_{\rm T} = v_N - v_{\rm T}, \tag{5}$$
$$\dot{v}_{\rm T} = u_{\rm T}, \tag{6}$$

where $u_{\rm T} \in \mathbb{R}$ is the control input of the T-CAV. By designing control laws for (4) and (6), we aim to stabilize the mixed traffic system. In addition, we seek formal safety guarantees for both CAVs by integrating their controllers with CBFs.

III. Stabilizing Controller Design

In this section, we first present a general controller for the two CAVs by extending the controller introduced in [9]. Then we analyze plant and string stability.

A. Nonlinear controller design

We assume that the two CAVs can measure their own gap, their own speed, and the speed of their preceding vehicle by on-board sensors. Furthermore, they can obtain the speed and position of each other via vehicle-to-vehicle (V2V) communication. The states of some of the middle HVs may also be available to the CAVs if they are equipped with communication devices. For each CAV, its controller consists of three parts: adaptive cruise control based on its preceding vehicle, state feedback using middle HVs' state, and coupling with another CAV. For the head CAV, its controller $u_{\rm H}$ is:

$$\begin{aligned} u_{\rm H} =& \alpha_{\rm H}(V_{\rm H}(s_{\rm H}) - v_{\rm H}) + \beta_{\rm H,d}(W(v_{\rm d}) - v_{\rm H}) \\ &+ \sum_{i=1}^{n_1} \beta_{{\rm H},i}(W(v_i) - v_{\rm H}) + \beta_{\rm H,T}(W(v_{\rm T}) - v_{\rm H}), \end{aligned} \tag{7}$$

where $\beta_{\rm H,d}$, $\beta_{{\rm H},i}$, and $\beta_{\rm H,T}$ are the control gains with respect to the speeds of the HHV, middle HVs, and the tail CAV, respectively. The function $W : \mathbb{R} \to \mathbb{R}$ is defined as:

$$W(v) = \min\{v, v_{\max}\}, \tag{8}$$

with $v_{\max} \in \mathbb{R}$ being the maximum speed. The control gain $\alpha_{\rm H}$ adjusts the head CAV's acceleration with respect to the desired speed $V_{\rm H}(s_{\rm H})$ based on the gap $s_{\rm H}$. We use $1 \le n_1 \le N$ to represent that n_1 HVs are within the H-CAV's communication range. If HV-i is not connected and the CAV cannot obtain its speed, then the CAV does not respond to it, i.e., the corresponding control gain becomes $\beta_{{\rm H},i} = 0$.

The tail CAV's acceleration is controlled as:

$$\begin{aligned} u_{\rm T} =& \alpha_{\rm T}(V_{\rm T}(s_{\rm T}) - v_{\rm T}) \\ &+ \sum_{i=n_2}^{N} \beta_{{\rm T},i}(W(v_i) - v_{\rm T}) + \beta_{\rm T,H}(W(v_{\rm H}) - v_{\rm T}), \end{aligned} \tag{9}$$

where $\alpha_{\rm T}$, $\beta_{{\rm T},i}$, and $\beta_{\rm T,H}$ are the controller gains, and $1 \le n_2 \le N$. If HV-i is not connected to or detected by the tail CAV, we have $\beta_{{\rm T},i} = 0$. For the gap-dependent desired speed, we take $V_{\rm H}(s)$ and $V_{\rm T}(s)$ as the following range policy:

$$V(s) = \begin{cases} 0, & s \le s_{\rm st}, \\ v_{\max}\frac{s - s_{\rm st}}{s_{\rm go} - s_{\rm st}}, & s_{\rm st} < s < s_{\rm go}, \\ v_{\max}, & s \ge s_{\rm go}, \end{cases} \tag{10}$$

where $s_{\rm st}$ and $s_{\rm go}$ are the standstill gap and free-driving gap.

B. Linear stability analysis

In this subsection, we analyze the stability of mixed traffic in the Laplace domain after linearization. The results reflect the local linear stability performance, i.e., when there are small perturbations around an equilibrium state.

We first linearize the mixed-autonomy system (1)-(6) around the equilibrium. At the equilibrium state, the vehicle chain drives at a uniform speed $v^* \in \mathbb{R}$. The HVs keep the gap $s_i^* \in \mathbb{R}$ decided by $F_i(s_i^*, v^*, 0) = 0$. We take small perturbations around the equilibrium as $\tilde{v}_i = v_i - v^*$ and $\tilde{s}_i = s_i - s_i^*$. The HV dynamics (1)-(2) are linearized as

$$\dot{\tilde{s}}_i = \tilde{v}_{i-1} - \tilde{v}_i, \tag{11}$$
$$\dot{\tilde{v}}_i = a_{i1}\tilde{s}_i - a_{i2}v_i + a_{i3}v_{i-1}, \tag{12}$$

with $a_{i1} = \frac{\partial F_i(s_i^*, v^*, 0)}{\partial s_i}$, $a_{i2} = \frac{\partial F_i(s_i^*, v^*, 0)}{\partial \dot{s}_i} - \frac{\partial F_i(s_i^*, v^*, 0)}{\partial v_i}$, $a_{i3} = \frac{\partial F_i(s_i^*, v^*, 0)}{\partial \dot{s}_i}$. The head CAV drives at the equilibrium speed $v^* < v_{\max}$ and keeps a gap $s_{\rm H}^*$ that can be designed according to $V_{\rm H}(s_{\rm H}^*) = v^*$. We take the state perturbations as $\tilde{s}_{\rm H} = s_{\rm H} - s_{\rm H}^*$, $\tilde{v}_{\rm H} = v_{\rm H} - v^*$, and the linearized dynamics:

$$\dot{\tilde{s}}_{\rm H} = \tilde{v}_{\rm d} - \tilde{v}_{\rm H}, \tag{13}$$
$$\dot{\tilde{v}}_{\rm H} = \tilde{u}_{\rm H}, \tag{14}$$

where the controller is

$$\tilde{u}_{\rm H} = \xi_{\rm H}\tilde{s}_{\rm H} + \eta_{\rm H}\tilde{v}_{\rm H} + \beta_{\rm H,d}\tilde{v}_{\rm d} + \sum_{i=1}^{n_1} \beta_{{\rm H},i}\tilde{v}_i + \beta_{\rm H,T}\tilde{v}_{\rm T}, \tag{15}$$

with $\xi_{\rm H} = \alpha_{\rm H}V_{\rm H}'(s_{\rm H}^*)$, $\eta_{\rm H} = -\alpha_{\rm H} - \beta_{\rm H,d} - \sum_{i=1}^{n_1}\beta_{{\rm H},i} - \beta_{\rm H,T}$. The tail CAV drives at the speed v^* and keeps a gap $s_{\rm T}^* \in \mathbb{R}$ designed via $V_{\rm T}(s_{\rm T}^*) = v^*$. With the perturbations $\tilde{s}_{\rm T} = s_{\rm T} - s_{\rm T}^*$, $\tilde{v}_{\rm T} = v_{\rm T} - v^*$, the linearized dynamics are:

$$\dot{\tilde{s}}_{\rm T} = \tilde{v}_N - \tilde{v}_{\rm T}, \tag{16}$$
$$\dot{\tilde{v}}_{\rm T} = \tilde{u}_{\rm T}, \tag{17}$$

where the controller is:

$$\tilde{u}_{\rm T} = \xi_{\rm T}\tilde{s}_{\rm T} + \eta_{\rm T}\tilde{v}_{\rm T} + \sum_{i=n_2}^{N} \beta_{{\rm T},i}\tilde{v}_i + \beta_{\rm T,H}\tilde{v}_{\rm H}, \tag{18}$$

with $\xi_{\mathrm{T}} = \alpha_{\mathrm{T}} V_{\mathrm{T}}'(s_{\mathrm{T}}^*)$, $\eta_{\mathrm{T}} = -\alpha_{\mathrm{T}} - \sum_{i=n_2}^{N} \beta_{\mathrm{T},i} - \beta_{\mathrm{T,H}}$.

We analyze stability based on the *head-to-tail transfer function* [18] defined as:

$$G(s) = \frac{\widetilde{V}_{\mathrm{T}}(s)}{\widetilde{V}_{\mathrm{d}}(s)}, \tag{19}$$

with $\widetilde{V}_{\mathrm{d}}(s)$ and $\widetilde{V}_{\mathrm{T}}(s)$ being the Laplace transforms of the speed perturbations of the head HV, $\tilde{v}_{\mathrm{d}}$, and the tail CAV, $\tilde{v}_{\mathrm{T}}$, respectively. For the linearized system, its head-to-tail transfer function $G(s)$ is given as in (20).

Lemma 1. *The head-to-tail transfer function is*

$$G(s) = \frac{(\beta_{\mathrm{H,d}} s + \xi_{\mathrm{H}})\phi_{\mathrm{T}}}{(s^2 - \eta_{\mathrm{T}} s + \xi_{\mathrm{T}})\phi_{\mathrm{H}} - \beta_{\mathrm{H,T}} s \phi_{\mathrm{T}}}, \tag{20}$$

where

$$\phi_{\mathrm{H}} = (s^2 - \eta_{\mathrm{H}} s + \xi_{\mathrm{H}})\Omega_0 - \sum_{i=1}^{n_1} \beta_{\mathrm{H},i} s \Omega_i, \tag{21}$$

$$\phi_{\mathrm{T}} = \beta_{\mathrm{T,H}} s \Omega_0 + \xi_{\mathrm{T}} \Omega_N + \sum_{i=n_2}^{N} \beta_{\mathrm{T},i} s \Omega_i, \tag{22}$$

with $\Omega_0 = \prod_{i=1}^{N} (s^2 + a_{i2} s + a_{i1})$,

$$\Omega_i = \prod_{j=1}^{i} (a_{j3} s + a_{j1}) \prod_{j=i+1}^{N} (s^2 + a_{j2} s + a_{j1}), \tag{23}$$

for $0 < i < N$, *and* $\Omega_N = \prod_{i=1}^{N} (a_{i3} s + a_{i1})$.

We analyze the stability of the mixed-autonomy traffic system with respect to two types of stability notions: *plant stability* and *heat-to-tail string stability*.

Plant stability: Plant stability requires that each vehicle's state can converge to the equilibrium value. The system is plant stable if all characteristic roots of $D(s) = 0$ have negative real parts with $D(s)$ being the denominator of the transfer function $G(s)$. The system is at the plant-stability boundary when $D(s) = 0$ has a real root $s = 0$ or has a complex conjugate pair of roots $s = \pm \mathrm{j}\omega$ with $\mathrm{j}^2 = -1$ and $\omega > 0$. For the first case, the stability boundary is:

$$D(0) = 0. \tag{24}$$

For the second case, the stability boundary is given as:

$$\mathrm{Re}(D(\mathrm{j}\omega)) = 0, \tag{25}$$

$$\mathrm{Im}(D(\mathrm{j}\omega)) = 0, \tag{26}$$

with $\mathrm{Re}(\cdot)$ and $\mathrm{Im}(\cdot)$ representing the real and imaginary parts of a complex number.

String stability: String stability requires that perturbations are attenuated along the vehicle chain when the motion (i.e., speed) of the leading vehicle is perturbed. By designing CAV controllers to meet string stability, CAVs help to mitigate traffic congestion and smooth traffic. For the vehicle chain in Fig. 1, we use the commonly adopted notion of *head-to-tail string stability* [18], which requires that when the speed of the head HV fluctuates, the tail CAV must have a smaller speed perturbation. More precisely, the vehicle chain is considered head-to-trail string stable if

$$|G(\mathrm{j}\omega)| < 1, \quad \forall \omega > 0. \tag{27}$$

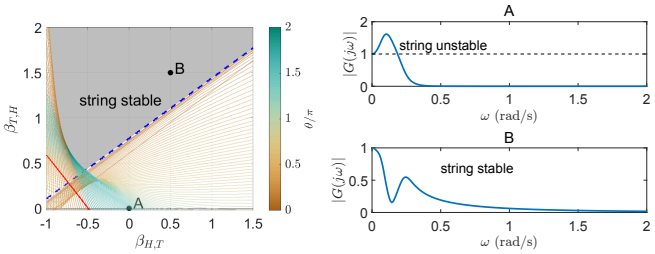

(a) Stability Chart (b) Frequency Response

Fig. 2: Stability chart of mixed autonomy-traffic with a CAV pair. When the two CAVs do not respond to each other (see point A with $\beta_{\mathrm{H,T}} = \beta_{\mathrm{T,H}} = 0$), the system is head-to-tail string unstable. The system becomes string stable after adding coupling terms in the controller (point B).

We note that $|G(0)| = 1$, and that there are two cases for the string stability boundaries. In the first case, the maximum of $|G(\mathrm{j}\omega)|$ is at $\omega = 0$, and the stability boundary is given as:

$$\lim_{\omega \to 0^+} P(\omega) = 0, \tag{28}$$

according to [9], where

$$P(\omega) = \frac{1}{\omega^2}(|D(\mathrm{j}\omega)|^2 - |N(\mathrm{j}\omega)|^2), \tag{29}$$

and $N(\mathrm{j}\omega)$ is the numerator of the transfer function $G(\mathrm{j}\omega)$. In the second case, we have $|G(\mathrm{j}\omega)| = 1$ for some positive ω. The stability boundary is a family of curves parameterized by the wave number $\theta \in [0, 2\pi)$ [9], obtained from

$$G(\mathrm{j}\omega) = e^{-\mathrm{j}\theta}, \tag{30}$$

which is equivalent to

$$\mathrm{Re}(D(\mathrm{j}\omega)) - \mathrm{Re}(N(\mathrm{j}\omega))\cos\theta + \mathrm{Im}(N(\mathrm{j}\omega))\sin\theta = 0, \tag{31}$$

$$\mathrm{Im}(D(\mathrm{j}\omega)) - \mathrm{Re}(N(\mathrm{j}\omega))\sin\theta - \mathrm{Im}(N(\mathrm{j}\omega))\cos\theta = 0. \tag{32}$$

As discussed below, these stability boundaries can be expressed as functions of the CAVs' control gains, which facilitates stabilizing control design.

C. Stability chart

As a result of stability analysis, we plot *stability charts*, which show the stability boundaries in the space of controller parameters and distinguish those parameters that make the system stable, ultimately enabling stabilizing control design.

We consider a vehicle chain with $N = 4$ middle HVs. For the human driver model F_i in (2), we implement the optimal velocity model (OVM):

$$F_i(s_i, \dot{s}_i, v_i) = \alpha\,(V(s_i) - v_i) + \beta \dot{s}_i. \tag{33}$$

The first term reflects how human drivers accelerate to match the desired gap-dependent speed $V(s)$, and the second term represents how human drivers accelerate based on the speed difference. We let $V(s)$ be the same for HVs as the CAVs' spacing policy in (10), and we set the parameters as: $\alpha = 0.3$ s^{-1}, $\beta = 0.6$ s^{-1}, $s_{\mathrm{st}} = 5$ m, $s_{\mathrm{go}} = 30$ m and $v_{\max} = 35$ m/s. We set the equilibrium speed as $v^* = 20$ m/s, and we obtain the equilibrium gap from $V(s^*) = v^*$ as $s^* \approx 19$ m for both HVs and CAVs. We take the controller gains as

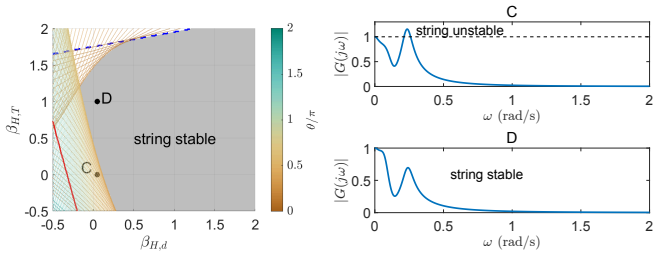

(a) Stability chart (b) Frequency Response

Fig. 3: Stability chart with $\beta_{\mathrm{T,H}} = 1.5$. The head CAV's response to the tail CAV can help achieve string stability (see points C with $\beta_{\mathrm{H,T}} = 0$ and D with $\beta_{\mathrm{H,T}} \neq 0$).

$\alpha_{\mathrm{H}} = 0.3\ \mathrm{s}^{-1}$, $\beta_{\mathrm{H,d}} = 0.5\ \mathrm{s}^{-1}$, $\beta_{\mathrm{H},i} = 0.1\ \mathrm{s}^{-1}$, $\alpha_{\mathrm{T}} = 0.2\ \mathrm{s}^{-1}$, $\beta_{\mathrm{T},i} = 0$ for $i = 1, 2, 3$, and $\beta_{\mathrm{T},N} = 0.4\ \mathrm{s}^{-1}$.

In Fig. 2, we plot the stability chart in the $(\beta_{\mathrm{H,T}}, \beta_{\mathrm{T,H}})$ domain. In particular, for the linearized system, we have

$$D(0) = \alpha_{\mathrm{T}}\alpha_{\mathrm{H}} V_{\mathrm{H}}'(s_{\mathrm{H}}^*) V_{\mathrm{T}}'(s_{\mathrm{T}}^*) \Pi_{i=1}^{N} a_{i1}, \tag{34}$$

which shows that $D(0)$ is independent of $\beta_{\mathrm{H,T}}$ and $\beta_{\mathrm{T,H}}$. Thus we ignore the plant stability boundary with $\omega = 0$ in (24). To plot the other stability boundaries, we first note that both $\mathrm{Re}(D(\mathrm{j}\omega))$, $\mathrm{Im}(D(\mathrm{j}\omega))$, $\mathrm{Re}(N(\mathrm{j}\omega))$ and $\mathrm{Im}(N(\mathrm{j}\omega))$ are linear with respect to $\beta_{\mathrm{H,T}}$ and $\beta_{\mathrm{T,H}}$. For the plant stability boundary with $\omega > 0$, we express $\beta_{\mathrm{H,T}}$ and $\beta_{\mathrm{T,H}}$ from (25)-(26) and get the boundary parameterized by ω as the red line in Fig. 2. The region above the red line represents controller gains that satisfy the plant stability condition. For example, the gains at points A and B both achieve plant stability.

For the string stability boundary with $\omega = 0$, we solve (28) for $\beta_{\mathrm{H,T}}$, $\beta_{\mathrm{T,H}}$, and get the dashed blue line in Fig. 2. For the string stability boundary with $\omega > 0$, we solve (31)-(32) for $\beta_{\mathrm{H,T}}$ and $\beta_{\mathrm{T,H}}$, which yields a curve parameterized by ω for each value of θ. The thin curves represent the string stability boundaries for each θ with the color bar from brown to green indicating the value of θ. The region of controller gains that render the mixed-autonomy traffic head-to-tail string stable is the grey-shaded area enclosed by these curves. For example, the controller of point B achieves string stability and attenuates perturbations along the vehicle chain, while point A causes string unstable behavior, as demonstrated also by the frequency response plots on the right; cf. (27). Importantly, string stability cannot be achieved if the two CAVs do not respond to each other (i.e., if $\beta_{\mathrm{H,T}} = \beta_{\mathrm{T,H}} = 0$).

In Fig. 3, we plot the stability chart in the $(\beta_{\mathrm{H,d}}, \beta_{\mathrm{H,T}})$ domain. We see that the response of the head CAV to the tail CAV with a proper choice of $\beta_{\mathrm{H,T}}$ gain can enlarge the range of $\beta_{\mathrm{H,d}}$ gains that achieve string stability. This is also highlighted by points C and D, which are both plant stable, and point C with $\beta_{\mathrm{H,T}} = 0$ is string unstable, while point D with $\beta_{\mathrm{H,T}} \neq 0$ is string stable.

IV. Safety-critical Control via CBFs

In this section, we first introduce CBFs, and then utilize them to design safety filters for the two CAVs.

A. Preliminaries on CBFs

Consider an affine control system with state $x \in \mathcal{D} \subset \mathbb{R}^n$ and control input $u \in \mathcal{U} \subset \mathbb{R}^m$:

$$\dot{x} = f(x) + g(x)u, \tag{35}$$

with f and g being locally Lipschitz. The system is safe if its state stays in a safe set $\mathcal{C}$, i.e, $x \in \mathcal{C}$. Let $\mathcal{C}$ be the 0-superlevel set of a continuously differentiable function $h : \mathcal{D} \to \mathbb{R}$:

$$\mathcal{C} = \{x \in \mathbb{R}^n : h(x) \geq 0\}. \tag{36}$$

Definition 1 (Control Barrier Function [2])**.** *Function h is called a control barrier function for the system* (35) *on $\mathcal{C}$ if there exists an extended class-$\mathcal{K}_\infty$ function γ such that*

$$\sup_{u \in \mathcal{U}} L_f h(x) + L_g h(x) u \geq -\gamma(h(x)), \quad \forall x \in \mathcal{C}, \tag{37}$$

with $L_f h = \nabla h(x) \cdot f(x)$ and $L_g h = \nabla h(x) \cdot g(x)$.

The CBF is used to guarantee safety as in Theorem 1.

Theorem 1 (Safety guarantee by CBF [2])**.** *If h is a control barrier function for* (35) *on $\mathcal{C}$, then any locally Lipschitz continuous controller u satisfying*

$$L_f h(x) + L_g h(x) u \geq -\gamma(h(x)), \quad \forall x \in \mathcal{C}, \tag{38}$$

renders the set $\mathcal{C}$ forward invariant (safe), i.e, $x(t) \in \mathcal{C}$, $\forall t \geq 0$ holds for the closed-loop system for all $x(0) \in \mathcal{C}$.

To control a system with formal safety guarantees, CBFs can be integrated with a pre-designed nominal controller u_0. In particular, the nominal control input can be modified in a minimal way to synthesize a safety-critical control input, by solving the quadratic program (QP):

$$\begin{aligned} u = \underset{u \in \mathbb{R}^m}{\operatorname{argmin}} \ & \|u - u_0\|^2, \\ \text{s.t. } & L_f h(x) + L_g h(x) u + \gamma(h(x)) \geq 0, \end{aligned} \tag{39}$$

that is also referred as *safety filter*. The QP has an explicit solution given by the Karush–Kuhn–Tucker (KKT) conditions:

$$u = \begin{cases} u_0, & \psi(x) \geq 0, \\ u_0 - \dfrac{\psi(x) L_g h(x)^\top}{L_g h(x) L_g h(x)^\top}, & \psi(x) < 0, \end{cases} \tag{40}$$

where $\psi(x) = L_f h(x) + L_g h(x) u_0 + \gamma(h(x))$. When the control input is a scalar, i.e., $u \in \mathbb{R}$, and $L_g h(x) < 0$ for all x, the solution (40) is equivalent to the more concise form:

$$u = \min \left\{ u_0, -\frac{L_f h(x) + \gamma(h(x))}{L_g h(x)} \right\}. \tag{41}$$

B. Safety filters for CAVs via CBFs

Now we use CBFs to ensure formal guarantees of safety for the CAVs w.r.t. front-end collisions. We adopt the constant time headway (CTH) safe spacing policy from [19]. For a vehicle with speed v and gap s, CTH requires:

$$s \geq \tau v, \tag{42}$$

where $\tau > 0$ is the safe time headway.

To apply the CTH by CBFs, we define the safety function:

$$h(x) = s - \tau v. \tag{43}$$

For the head CAV dynamics (3)-(4), that are associated with $x = \begin{bmatrix} s_{\mathrm{H}} & v_{\mathrm{H}} \end{bmatrix}^\top$, $f(x) = \begin{bmatrix} v_{\mathrm{d}} - v_{\mathrm{H}} & 0 \end{bmatrix}^\top$ and $g(x) = \begin{bmatrix} 0 & 1 \end{bmatrix}^\top$,

TABLE I: Four types of controllers for the two CAVs

	H-CAV Nominal (7)	H-CAV CBF (44)
T-CAV Nominal (9)	I	II
T-CAV CBF (45)	III	IV

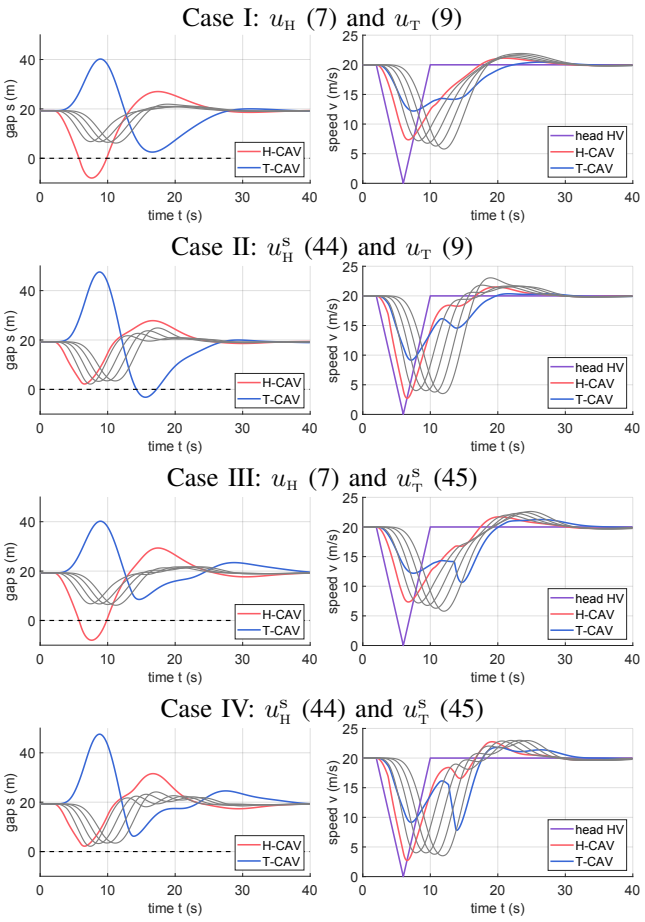

Fig. 4: Simulation of the proposed safety-critical traffic controllers. Nominal stabilizing controllers yield string stability, and CBFs-based safety filters on both CAVs ensure safety.

the safety function h in (43) provides the safety-critical control input $u_{\rm H}^{\rm s} \in \mathbb{R}$ via (41) as:

$$u_{\rm H}^{\rm s} = \min\left\{u_{\rm H}, \frac{v_{\rm d} - v_{\rm H} + \gamma_{\rm H}(s_{\rm H} - \tau_{\rm H} v_{\rm H})}{\tau_{\rm H}}\right\}. \tag{44}$$

Here, $u_{\rm H}$ is the nominal stabilizing controller in (7). Similarly, the safety-critical input $u_{\rm T}^{\rm s} \in \mathbb{R}$ for the tail CAV is:

$$u_{\rm T}^{\rm s} = \min\left\{u_{\rm T}, \frac{v_N - v_{\rm T} + \gamma_{\rm T}(s_{\rm T} - \tau_{\rm T} v_{\rm T})}{\tau_{\rm T}}\right\}. \tag{45}$$

C. Safety and stability performance analysis

We run simulations to study the performance of the proposed safety-critical controllers. We use the parameters in Section III-C. A safety-critical scenario is considered in which the HHV suddenly decelerates. This may be caused in real traffic by an aggressive cut-in or a pedestrian. We set the HHV's acceleration as:

$$\dot{v}_{\rm d} = \begin{cases} -a_{\rm d}, & t \in [2, 2 + \Delta v_{\rm d}/a_{\rm d}], \\ a_{\rm d}, & t \in (2 + \Delta v_{\rm d}/a_{\rm d}, 2 + 2\Delta v_{\rm d}/a_{\rm d}], \\ 0, & \text{otherwise}, \end{cases} \tag{46}$$

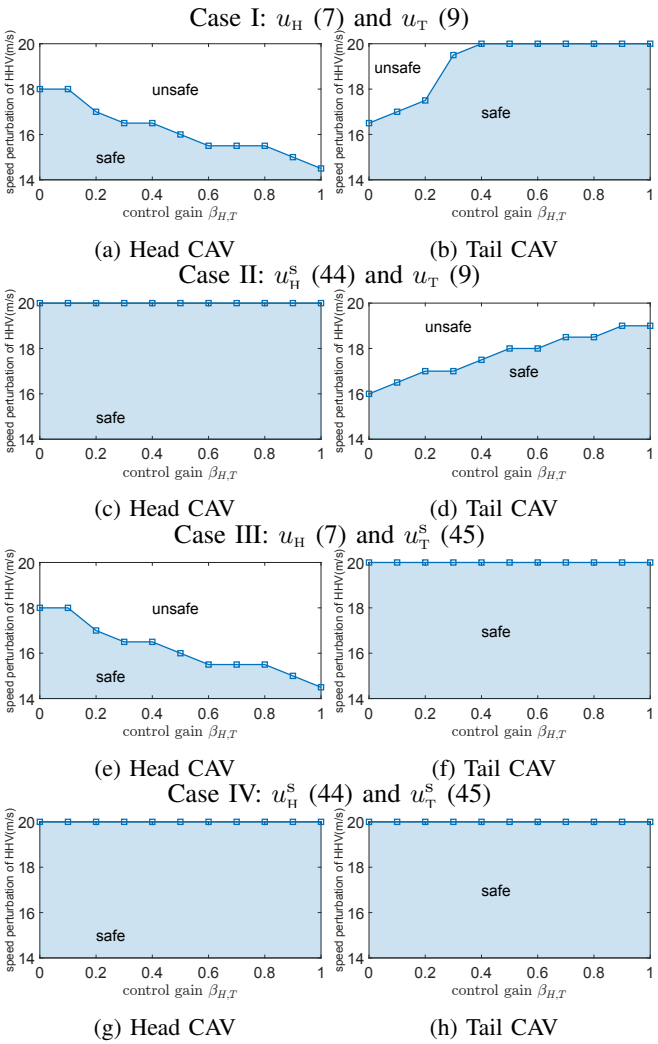

Fig. 5: The range of speed perturbations of the HHV that causes no collisions for the following CAVs.

where $a_{\rm d}$ is HHV's acceleration, $\Delta v_{\rm d}$ is the speed perturbation of HHV, and $\Delta v_{\rm d}/a_{\rm d}$ is the duration of deceleration.

Figure 4 shows the simulated response of the vehicle chain by plotting the profiles of gap s and speed v for $a_{\rm d} = 5$ m/s^2 and $\Delta v_{\rm d} = 20$ m/s. We compare four cases, highlighted in Table I, depending on whether the head and tail CAVs use the nominal or the safety-critical controller. When both CAVs use nominal controllers in Fig. 4(a), they achieve head-to-tail string stability, but the head CAV collides with the HHV. By using safety filter on the head CAV in Fig. 4(b), it avoids collisions, but there is a collision for the tail CAV that runs the nominal controller. By using safety filter on the tail CAV only, the head CAV remains unsafe in Fig. 4(c). Finally, using CBF-based safety filters on both CAVs in Fig. 4(d) successfully achieves safety for both. Remarkably, head-to-tail string stability is still observed as the tail CAV reduces its speed much less than the HHV.

After repeating these simulations with various parameters, Fig. 5 highlights the range of HHV speed perturbations that causes no collision ($s \geq 0$) for the CAVs, as a function of the nominal controller gain $\beta_{\rm H,T}$. The safe region in Fig. 5 shows that using CBFs to maintain safety for the head CAV

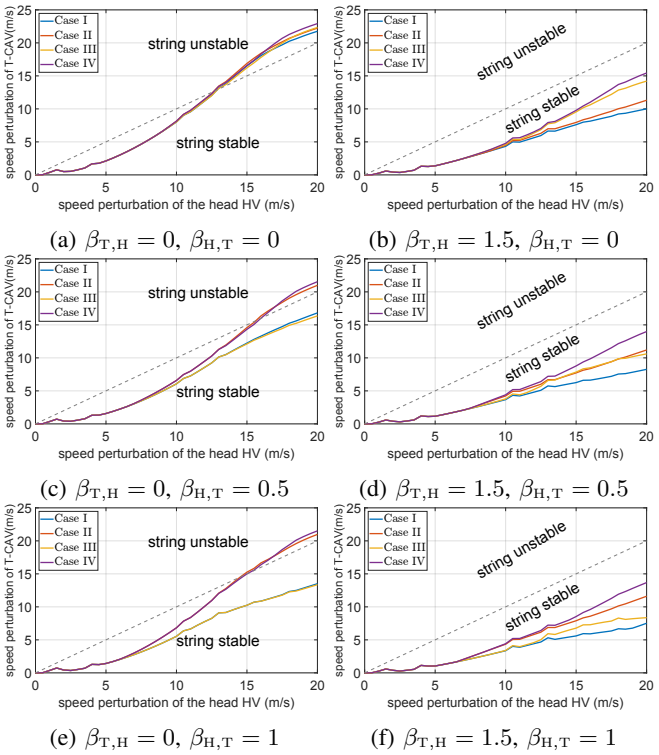

(a) $\beta_{\mathrm{T,H}} = 0$, $\beta_{\mathrm{H,T}} = 0$ (b) $\beta_{\mathrm{T,H}} = 1.5$, $\beta_{\mathrm{H,T}} = 0$

(c) $\beta_{\mathrm{T,H}} = 0$, $\beta_{\mathrm{H,T}} = 0.5$ (d) $\beta_{\mathrm{T,H}} = 1.5$, $\beta_{\mathrm{H,T}} = 0.5$

(e) $\beta_{\mathrm{T,H}} = 0$, $\beta_{\mathrm{H,T}} = 1$ (f) $\beta_{\mathrm{T,H}} = 1.5$, $\beta_{\mathrm{H,T}} = 1$

Fig. 6: Speed perturbation of the head HV and the tail CAV. The mixed traffic vehicle chain is string stable if the tail CAV has a smaller speed perturbation than the HHV.

may cause collisions for the tail CAV if it uses the nominal controller, but not vice versa. When both CAVs use safety-critical controllers, there are no collisions.

To analyze how the CBFs affect string stability, we compare the speed perturbation of the tail CAV $\Delta v_{\mathrm{T}} = \max_{t\geq 0} v_{\mathrm{T}}(t) - \min_{t\geq 0} v_{\mathrm{T}}(t)$ to that of the HHV Δv_{d} in Fig. 6 for simulations with various controller gains $\beta_{\mathrm{H,T}}$ and $\beta_{\mathrm{T,H}}$. We see from Fig. 6(a) that the nominal controller causes string unstable behavior ($\Delta v_{\mathrm{T}} \geq \Delta v_{\mathrm{d}}$) when the two CAVs do not respond to each other, i.e., $\beta_{\mathrm{T,H}} = \beta_{\mathrm{H,T}} = 0$. When the two CAVs leverage connectivity and respond to each other as proposed, the nominal controller achieves string stable driving. For certain control gains, the safety-critical traffic controllers may sacrifice string stability for safety; see Fig. 6(c,e). However, well-designed safety-critical traffic controllers, shown in Fig. 6(b,d,f), can both achieve string stability and guarantee safety. This highlights the potential of the proposed safety-critical traffic stabilization method by CAV pairs to ensure safe and smooth mobility on highways.

V. Conclusion

In this paper, we proposed a safety-critical design framework for controlling mixed-autonomy traffic by a pair of connected and automated vehicles (CAVs). The CAVs travel within each other's communication range amongst human drivers. We designed nominal controllers for the CAVs to cooperatively achieve head-to-tail string stability and thereby mitigate traffic congestion. Control barrier functions were used to minimally modify these controllers to formally guarantee safety w.r.t. front-end collision. Finally, we demonstrated safety and string stability in mixed traffic by numerical simulations, and highlighted the benefits of connectivity between the CAV pair.

References

[1] M. Althoff and J. M. Dolan, "Online verification of automated road vehicles using reachability analysis," *IEEE Transactions on Robotics*, vol. 30, no. 4, pp. 903–918, 2014.

[2] A. D. Ames, S. Coogan, M. Egerstedt, G. Notomista, K. Sreenath, and P. Tabuada, "Control barrier functions: Theory and applications," in *18th European Control Conference*. IEEE, 2019, pp. 3420–3431.

[3] A. D. Ames, J. W. Grizzle, and P. Tabuada, "Control barrier function based quadratic programs with application to adaptive cruise control," in *53rd IEEE Conference on Decision and Control*. IEEE, 2014, pp. 6271–6278.

[4] M. Čičić, X. Xiong, L. Jin, and K. H. Johansson, "Coordinating vehicle platoons for highway bottleneck decongestion and throughput improvement," *IEEE Transactions on Intelligent Transportation Systems*, vol. 23, no. 7, pp. 8959–8971, 2021.

[5] S. Cui, B. Seibold, R. Stern, and D. B. Work, "Stabilizing traffic flow via a single autonomous vehicle: Possibilities and limitations," in *IEEE Intelligent Vehicles Symposium*. IEEE, 2017, pp. 1336–1341.

[6] M. L. Cunningham, M. A. Regan, S. A. Ledger, and J. M. Bennett, "To buy or not to buy? Predicting willingness to pay for automated vehicles based on public opinion," *Transportation Research Part F: Traffic Psychology and Behaviour*, vol. 65, pp. 418–438, 2019.

[7] C. M. Gisolo, M. L. Delle Monache, F. Ferrante, and P. Frasca, "Nonlinear analysis of stability and safety of optimal velocity model vehicle groups on ring roads," *IEEE Transactions on Intelligent Transportation Systems*, vol. 23, no. 11, pp. 20 628–20 635, 2022.

[8] S. Gong and L. Du, "Cooperative platoon control for a mixed traffic flow including human drive vehicles and connected and autonomous vehicles," *Transportation Research Part B: Methodological*, vol. 116, pp. 25–61, 2018.

[9] S. Guo, G. Orosz, and T. G. Molnar, "Connected cruise and traffic control for pairs of connected automated vehicles," *IEEE Transactions on Intelligent Transportation Systems*, vol. 24, no. 11, pp. 12 648–12 658, 2023.

[10] M. Krstic, "Inverse optimal safety filters," *IEEE Transactions on Automatic Control*, vol. 69, no. 1, pp. 16–31, 2024.

[11] V.-A. Le, H. M. Wang, G. Orosz, and A. A. Malikopoulos, "Coordination for connected automated vehicles at merging roadways in mixed traffic environment," in *2023 62nd IEEE Conference on Decision and Control (CDC)*. IEEE, 2023, pp. 4150–4155.

[12] I. M. Mitchell, A. M. Bayen, and C. J. Tomlin, "A time-dependent Hamilton-Jacobi formulation of reachable sets for continuous dynamic games," *IEEE Transactions on Automatic Control*, vol. 50, no. 7, pp. 947–957, 2005.

[13] T. G. Molnár, M. Hopka, D. Upadhyay, M. Van Nieuwstadt, and G. Orosz, "Virtual rings on highways: Traffic control by connected automated vehicles," in *AI-enabled Technologies for Autonomous and Connected Vehicles*. Springer, 2023, pp. 441–479.

[14] R. E. Stern, S. Cui, M. L. Delle Monache, R. Bhadani, M. Bunting, M. Churchill, N. Hamilton, H. Pohlmann, F. Wu, B. Piccoli *et al.*, "Dissipation of stop-and-go waves via control of autonomous vehicles: Field experiments," *Transportation Research Part C: Emerging Technologies*, vol. 89, pp. 205–221, 2018.

[15] J. Wang, Y. Lian, Y. Jiang, Q. Xu, K. Li, and C. N. Jones, "Distributed data-driven predictive control for cooperatively smoothing mixed traffic flow," *Transportation Research Part C: Emerging Technologies*, vol. 155, p. 104274, 2023.

[16] S. Wang, M. Shang, M. W. Levin, and R. Stern, "A general approach to smoothing nonlinear mixed traffic via control of autonomous vehicles," *Transportation Research Part C: Emerging Technologies*, vol. 146, p. 103967, 2023.

[17] W. Xiao, C. G. Cassandras, and C. A. Belta, "Bridging the gap between optimal trajectory planning and safety-critical control with applications to autonomous vehicles," *Automatica*, vol. 129, p. 109592, 2021.

[18] L. Zhang and G. Orosz, "Motif-based design for connected vehicle systems in presence of heterogeneous connectivity structures and time delays," *IEEE Transactions on Intelligent Transportation Systems*, vol. 17, no. 6, pp. 1638–1651, 2016.

[19] C. Zhao, H. Yu, and T. G. Molnar, "Safety-critical traffic control by connected automated vehicles," *Transportation Research Part C: Emerging Technologies*, vol. 154, p. 104230, 2023.